A contribution to simulating a three-dimensional larynx model using the finite element method

Marcelo de Oliveira Rosa[a] and José Carlos Pereira[b]
Depto. Engenharia Elétrica, Escola de Engenharia de São Carlos, Universidade de São Paulo, Av. Trabalhador sancarlense, 400, 13566-590, São Carlos, São Paulo, Brazil

Marcos Grellet
Depto. de Oftalmologia e Otorrinolaringologia, Faculdade de Medicina de Ribeirão Preto, Universidade de São Paulo, Av. Bandeirantes, 3900, 14049-900, Ribeirão Preto, São Paulo, Brazil

Abeer Alwan
Speech Processing and Auditory Perception Laboratory, Department of Electrical Engineering, 66-147E Engr. IV, 405 Hilgard Avenue, Box 951594, University of California, Los Angeles, California

(Received 3 January 2003; revised 14 August 2003; accepted 25 August 2003)

A three-dimensional model is presented to simulate the larynx during vocalization. The finite element method is used to calculate the airflow velocity and pressure along the larynx as well as tissue displacement. It is assumed that the larynx tissue is transversely isotropic and divided into three tissues: cover, ligament, and body. A contact-impact algorithm is incorporated to deal with the physics of the collision between both true vocal folds. The results show that the simulated larynx can reproduce the vertical and horizontal phase difference in the tissue movements and that the false vocal folds affect the pressure distribution over the larynx surfaces. The effects of exciting the larynx with different pressure drops are also investigated. © *2003 Acoustical Society of America.* [DOI: 10.1121/1.1619981]

PACS numbers: 43.70.Aj, 43.70.Bk, 43.70.Ep [AL] Pages: 2893–2905

I. INTRODUCTION

Larynx modeling is critical for providing insight into the dynamic behavior of human phonation. Using mathematical techniques and experimental data, models have been proposed in order to better understand how the larynx vibrates, what are its vibration conditions, and the influence of the tissue mechanics on the glottal and speech waveform. A better model of the larynx may also help in addressing two important clinical issues: Is it possible to predict a certain voice pathology based on a mathematical model of the larynx? Could a mathematical model simulate, *a priori*, the effects of a surgical intervention in a damaged larynx?

Several models have been proposed to deal with voice synthesis and larynx simulation. Ishizaka and Flanagan (1972), for example, present a very simple and efficient two-mass model where several aspects of normal phonation were investigated. Alipour *et al.* (2000), on the other hand, present a sophisticated larynx model where complex and rigorous mechanical and geometric characteristics of the tissues are applied in order to obtain a more realistic representation of the vocal fold dynamics. The advantage of continuum models is their ability to directly relate the geometric, viscoelastic, and aerodynamic characteristics of the larynx with the synthesized glottal waveform. In this paper, a three-dimensional finite element model of the larynx is proposed. The model builds and expands on that proposed by Alipour *et al.* (2000).

Three-dimensional larynx models are challenging in terms of computational efforts to solve the physical laws that control human phonation. The airflow pressure and velocities are described by Navier–Stokes equations while viscoelastic models deal with the larynx tissue movements. In addition, the collision of the vocal folds has an important impact on modeling because it affects the glottal waveform shape. The proposed model uses well-established algorithms to account for these three phenomena.

Berry *et al.* (1994) analyze the vibration pattern resulting from the simulation of a two-dimensional model of the vocal folds. They show that a nonchaotic pattern is found when the viscoelastic and aerodynamic conditions in the larynx are properly set. Berry and Titze (1996) state that tissue incompressibility is an important factor in the vibration modes. Both studies present sets of viscoelastic parameters of the larynx tissues for normal vibration.

De Vries *et al.* (1999) describes a three-dimensional model similar to Alipour's one. The only difference between both models is that De Vries *et al.* (1999) assume that the larynx tissues consist of body and cover tissues while Alipour *et al.* (2000) consider the body, ligament, and cover in their tissue formulation.

Alipour *et al.* (2000) present a three-dimensional model of a vocal fold (assuming larynx symmetry) where the longitudinal movements of the tissue model are restricted by assuming that these movements are negligible (the shear stress produced by the movements of successive transversal planes was incorporated in their formulation by algebraic manipulations). Additionally, the collision between the vocal folds are treated in their larynx model by bounding the tissue

[a]This work is part of the first author's Ph.D. thesis.
[b]Author to whom correspondence should be addressed. Electronic mail: pereira@sel.eesc.sc.usp.br

displacements: when their surface nodes cross the symmetry plane, they simply zero the nodal displacements in order to avoid the vocal folds penetrating into each other.

In terms of aerodynamic simulation, Guo and Scherer (1993) use a finite element model to determine the air velocity and pressure in a two-dimensional representation of the larynx channel (considering only the true vocal folds). They demonstrate that different laryngeal profiles significantly change the aerodynamic forces applied over the vocal fold surfaces.

The present model considers the whole larynx (including false vocal folds and laryngeal ventricles) in three dimensions and not just the true vocal folds. Hence, important vibration properties like the horizontal phase-difference can be studied. Following Alipour *et al.* (2000), the tissue model was linearly transversal isotropic because of the strain–stress differences in the longitudinal direction and transversal planes. However, the model assumes that the larynx moves longitudinally.

The aerodynamic influence of the false vocal folds is analyzed in order to demonstrate their influence in whispered voices as mentioned by Miller *et al.* (1988). In addition, the nonlinear pressure distribution calculated along the larynx surfaces allows us to confirm the myoelastic-aerodynamic theory. By solving the Navier–Stokes equation in three dimensions, the present model extends the Guo and Scherer one.

Finally, a physically based method to deal with the collision phenomenon is presented. It calculates the collision forces that avoid the larynx tissue interpenetration during phonation (Newton's second law). It is different from the two-mass model approach where the strain–stress relationship of the larynx tissue is changed during the collision, and from the Alipour *et al.* (2000) technique of direct manipulation of the surface tissue displacements.

The fundamental mathematical technique used in this work is the finite-element method which is a procedure of discretizing partial differential equations. Consequently, all the physical systems (fluid, tissue, and collision problem) involved in phonation are addressed by this technique. Descriptions of the finite-element algorithms are well-documented elsewhere (Bathe, 1996).

II. MATERIALS AND METHODS

The simulation of the larynx in phonatory conditions requires the solution of four different engineering problems: fluid flow, tissue displacement, mesh deforming, and contact problem. Because well-established algorithms are used to solve these problems, only ''how-to-use'' procedures will be addressed.

A. Mesh generator and deforming

Both airflow and tissue meshes are constructed from geometric specifications of the larynx. It is considered that the larynx is sliced into several cross sections along the neck. Therefore several small ''hyper-ellipses'' are specified to define both the internal and external larynx tissue surfaces—the internal tissue surface is the external flow channel. Figure 1 shows a geometric description of a larynx from its hyper-ellipses where the larynx surfaces are shown.

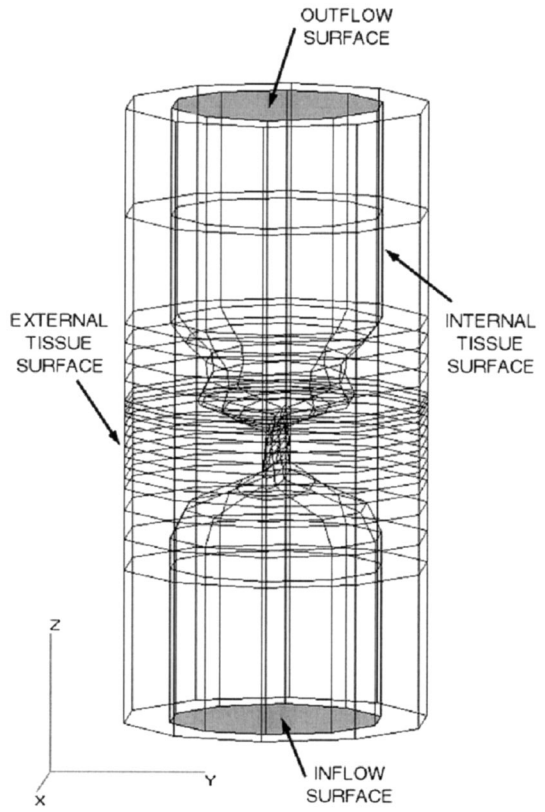

FIG. 1. Geometric description of the larynx surfaces from its hyper-elliptical sections.

The equations used to define all hyper-ellipses are

$$\begin{aligned} &x = R_1 \cos(\theta), \quad y = R_1 \sin(\theta), \quad 0 \leqslant \theta \leqslant \pi/2, \\ &x = R_2 \cos(\theta), \quad y = R_2 \sin(\theta), \quad \pi/2 \leqslant \theta \leqslant \pi, \\ &x = R_3 \cos(\theta), \quad y = R_3 \sin(\theta), \quad \pi \leqslant \theta \leqslant 3\pi/2, \\ &x = R_4 \cos(\theta), \quad y = R_4 \sin(\theta), \quad 3\pi/2 \leqslant \theta \leqslant 2\pi. \end{aligned} \tag{1}$$

To complete the tissue specification, the thickness of the larynx cover and ligament are defined—the remaining space between both internal and external tissue surfaces is considered as being part of the body layer. Later the geometric description of the laryngeal model will be presented.

Once these geometric characteristics are defined, an automatic mesh algorithm creates the tetrahedrons (polygonal elements used by FEM). At the airflow–muscle interface, both the flow and tissue elements are EXACTLY connected to each other by their triangular surfaces. It means that the airflow and tissues ''share'' the same nodes at their interfaces. In all simulations, the number of nodes for airflow and tissue meshes are 4151 and 5140, respectively. The numbers of tetrahedrons for airflow and tissue meshes are 2600 and 3000, respectively. The node and tetrahedron distribution in both meshes is determined by the spatial position of the hyper-ellipses: denser nodal distributions are obtained where successive hyper-ellipses are closer. The larynx movements demand that all of the larynx mesh moves. The position of all tissue nodes are naturally updated using the computed dis-

placements of the tissue FEM model. However, only the displacements of the external flow nodes are known because of their connection to nodes of the tissue surfaces.

The mesh moving technique of Johnson and Tezduyar (1994) is used to update the internal flow nodes. They considered that the flow mesh is a rigid material subject to specific displacements of all external nodes. Therefore the same FEM procedure used to model the larynx tissues is employed here. Specifically, tetrahedrons with linear polynomials for interpolation and shape functions are used. Because the ''material'' is isotropic, Johnson and Tezduyar (1994) defined the factor λ/μ_L (where λ and μ_L are Lamé elastic constants) as the only ''physical'' parameter for the mesh moving method. They proposed $\lambda/\mu_L = 2$ in order to control the deformation that is used in the mesh moving algorithm.

The boundary conditions of this algorithm are Dirichlet conditions and no body force is applied. Therefore only flow nodes in contact with the tissue ones have the same displacement. The displacement of inflow and outflow nodes are set to null.

This strategy provides a fast and reliable deformation of the flow mesh in several situations. At each simulation time step, the displacements of the external tissue nodes are collected and applied as boundary conditions to the mesh moving algorithm. It adequately places all internal flow nodes inside the larynx channel.

However, there are situations where this algorithm could not deal with the boundary conditions requirements. We noticed this phenomenon by examining the resulting mesh: some tetrahedrons had null or negative volumes. When this happens, the mesh generator is triggered to reconstruct all flow tetrahedrons from the deformed internal tissue surfaces.

B. Solving the tissue displacement

The concepts of continuum mechanics presented by Alipour *et al.* (2000) to describe tissue displacement during phonation are adopted. Thus, the simulated larynxes are divided into finite geometric elements and the displacement vectors and pressures are distributed throughout all the elements that compose the meshes.

It is assumed that the larynx tissues have transversal isotropic properties along the vocal fold length (longitudinal direction) attempting to match the fibrous directions of the laryngeal tissues. Mathematically the larynx tissues follow the linear elasticity theory, demanding therefore small time integration intervals as indicated by Alipour *et al.* (2000). The complete derivation of the element matrices involved in FEM will not be presented here because it can be found in Alipour *et al.* (2000), Huebner and Thornton (1982), and Bathe (1996).

However, there are some differences between our studies and Alipour *et al.* (2000) modeling. First, their model did not account for the longitudinal movements of the vocal folds in order to significantly reduce the number of equations whereas we analyze the magnitude of the movements in that direction. It is interesting to note that Alipour *et al.* (2000) coupled all the transversal planes through the use of shear forces. Here such forces are implicitly considered in the conventional and truly three-dimensional finite element modeling of the larynx tissues as in Gunter (2003).

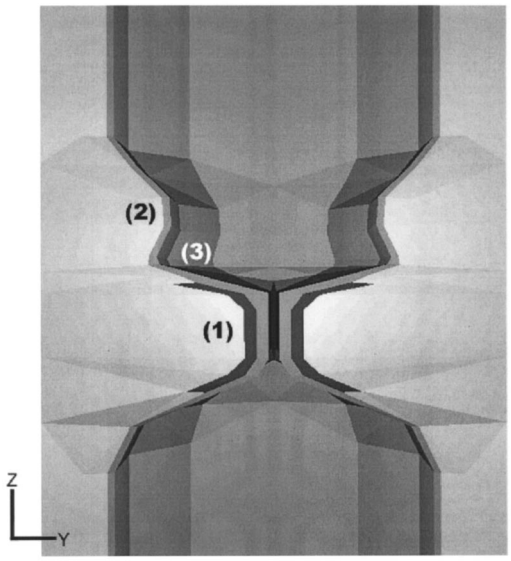

FIG. 2. Transversal view of a simulated normal larynx. The different shades refer to the three different tissues in the laryngeal tissue. (1) True vocal folds. (2) False vocal folds. (3) Laryngeal ventricles.

Second, their model—including Gunter (2003)—considered only the true vocal folds and it assumed symmetry of the right and left vocal folds. This allowed for the suppression of one of the folds in order to also reduce the number of equations to be solved. Figure 2 shows that the simulated larynx in this paper included both true and false vocal folds.

In terms of FEM, tetrahedrons are used to describe the tissue mesh. Different from Alipour *et al.* (2000), quadratic polynomials are employed as interpolation functions for displacement vectors and as shape functions for describing the geometry of the tetrahedrons. It is important to mention that straight-edged tetrahedrons are used to simplify the integral functions required to compute the element matrices in FEM. Although more accurate solutions are obtained with higher-order polynomials, the decision of using quadratic instead of linear elements was made to simplify numerical algorithms for both tissue and airflow modeling. Further explanations in the following subsection will justify the use of such interpolation and shape functions.

The boundary conditions that excite the tissue movements are air pressure at the internal surface of the larynx model (contact interface between air and tissue) and null displacement at all other external surfaces of the model. It means that the larynx is ''stuck'' at the neck during the entire phonation process. Specifically, the air pressures at the tissue nodes in contact with the airflow are linearly distributed along the external triangular surfaces. Air shear forces at the larynx walls are nulls because of the boundary conditions applied to solve the airflow model. Titze and Talkin (1979) pointed that these shear forces are very small when compared to the pressure forces, which justifies our assumption.

While Alipour *et al.* (2000) use a central difference approximation method to time-integrate the tissue equations, the Newmark method (Bathe, 1996) is used because of its

''unconditional'' stability. The time step (Δt) for all simulations is 300 μs. Its mathematical structure is implicit and produces a global linear system of equations to be solved. Therefore a direct sparse solver based on a supernodal approach (Demmel *et al.*, 1999) is employed.

The laryngeal tissue is divided into three kinds of tissues (cover, ligament, and body) following Alipour *et al.* (2000) and different from De Vries *et al.* (1999). These three kind of tissues differ from each other in terms of elastic constant, damping ratios, and geometric characteristics.

C. Solving the velocity-pressure flow

A laminar, incompressible, isothermal, steady Navier–Stokes equation (NS), as shown in Eq. (2), describes the airflow modeled by FEM. Although the larynx airflow is time dependent, the approach provided by Guo and Scherer (1993) is used in order to directly compare the results. In addition, it simplifies the mathematical description of the problems since the larynx movements should be incorporated into time-dependent airflow equations.

$$\nabla \cdot \mathbf{U} = 0,$$
$$\rho_f(\mathbf{U}\cdot\nabla)\mathbf{U} = \mu_f(\nabla^2\mathbf{U}) - \nabla\mathbf{P}, \tag{2}$$

where $\mathbf{U}$ is the velocity vector, $\mathbf{P}$ is the scalar pressure, and ρ_f and μ_f are the density and viscosity air, respectively.

The airflow mesh is divided into tetrahedrons (as in the tissue model) with quadratic and linear polynomials to respectively interpolate the velocity and pressure along the element (known as mixed formulation). This procedure is necessary to obtain a well-posed problem (Gresho and Sani, 1998). While Guo and Scherer (1993) use a penalty formulation, a mixed formulation of NS (using Lagrange multipliers) is adopted here.

To calculate the velocity and pressure along the larynx for several profiles, several strategies are applied in order to deal with the convergence difficulties for high-Reynolds number flows. These strategies are described in the next paragraphs.

One of the sources of difficulty is the convection term of NS. High-speed flows tend to produce ''wiggles'' that can destabilize the solution. One way to control this problem is to make the mesh finer. However, the drawback is the significant increase in the number of equations to be solved, specially in three dimensions.

A hybrid approach (FIDAP, 1999) is followed to obtain a robust FEM formulation of NS in high-Reynolds laminar flows by applying artificial numerical diffusion in the solution. It means that low- and high-order schemes are linearly combined to stabilize the convection term. Low-order schemes are first-order accurate and unconditionally stable but they introduce excessive amounts of numerical diffusion. On the other hand, high-order schemes (in our case, second-order accurate) significantly reduce numerical diffusion but are inherently unstable.

The first- and second-order schemes (the last is also called Streamline-Upwind/Petrov-Garlekin or SUPG) are respectively described by Tabata and Fujima (1991) and Sampaio (1991). Tabata and Fujima (1991) use triangles (with quadratic polynomials) while this work employs tetrahedrons (the adaptation between both geometric elements is direct). Sampaio (1991) also uses triangles but with linear polynomials for velocity. Deblois (1996) provides additional information to construct the element matrices associated to SUPG for triangles with quadratic polynomials for velocity (easily extended to tetrahedrons).

The blending procedure to mix both first- and second-order schemes follows FIDAP (1999) where the velocity gradient is locally evaluated by using a simple Laplacian filter applied over the faces of the analyzed tetrahedron. It produces a numerical estimation of the flow changes along the mesh and allows for quantifying the amount of both schemes (first- and second-order, respectively) used to construct all FEM element matrices. This hybrid approach is equivalent to finite-difference methods like MUSCL and TVD (Hirsh, 1988) in combining robustness (first-order schemes) and accuracy (high-order schemes).

To complete the problem specification, the boundary conditions are set to null velocity for external flow nodes in contact with tissue nodes. It means that the air velocities through the larynx wall are zero. Although these wall velocities should be not zero because of the tissue movements, they are considered zero in order to simplify the algorithms, specially when there is a collision between both true vocal folds. It is important to mention that tissue movements are significantly slower (approximately 100 times in the glottal channel) than the average airflow velocity, making the algorithm-based decision suitable for all simulations.

Pressures are set constant for the inflow and outflow larynx surfaces (respectively ''lungs'' and ''supraglottal'' pressures)—null velocity gradients are assumed at both surfaces. Therefore an aerodynamic condition is created to excite flow through the larynx using specific pressure drops between the inflow and outflow surfaces. Mathematically the ''do-nothing'' concept of Sani and Gresho (1994) is followed to keep the problem well-posed.

After the definition of the FEM approach to discretize NS for all finite elements (producing local nonlinear equation systems), a global nonlinear equation system to be solved is constructed. As Guo and Scherer (1993) the successive substitution method is used, i.e.,

$$K(\mathbf{U_{n-1}})\mathbf{U}^* = \mathbf{R},$$
$$\mathbf{U_n} = 0.5\mathbf{U_{n-1}} + 0.5\mathbf{U}^*, \tag{3}$$

where $\mathbf{U}^*$, $\mathbf{U_{n-1}}$, and $\mathbf{U_n}$ are global solution vectors (velocity+pressure) for temporary, $(n-1)$th and nth iteration steps. The solution is achieved when Eq. (4) is reached. A direct sparse solver (Demmel *et al.*, 1999) is used to solve the linear system in Eq. (3):

$$\frac{|\mathbf{U_n} - \mathbf{U_{n-1}}|}{|\mathbf{U_n}|} < 0.001. \tag{4}$$

The reduced basis method (Peterson, 1989) is used to speed up and control the convergence. The simulation is pressure driven and therefore large pressure drops (around 8 kdyne/cm^2) excite the flow in the larynx. Instead of fully applying this amount of pressure difference, a set of N sub-

problems at low pressure drops using Eq. (3) is solved. Once all these subsolutions (also called basis) have been determined, an approximate solution is finally calculated in order to form the first guess of the final iterative process to reach the correct solution, using again Eqs. (3) and (4). The following steps describe the reduced basis method:

(1) Estimate first base **U0th_base**
(2) Calculate additional basis **U1st_base...U4th_base**
(3) Calculate the final approximated solution **Ureduced_base**
(4) Converge up to the solution from **Usolved.**

$N=5$ was used to speed up convergence by quickly getting a good first guess (**Ureduced_base**). The choice for this value is a tradeoff between speed and computational efforts.

The final aspect in our method is the choice of the pressure drops for each subproblem. A simple approach is used: Starting from a specific pressure drop $\Delta P4$, $\Delta P0=\Delta P4/5$, $\Delta P1=2*\Delta P4/5$, $\Delta P2=3*\Delta P4/5$ and $\Delta P3=4*\Delta P4/5$.

Although we tried to mathematically define an association between $\Delta P4$ and parameters of the flow (Reynolds number, residue, $|\mathbf{U_n}-\mathbf{U_{n-1}}|$, etc.), it was finally decided to pick the parameter based on the convergence rate: low and high pressure drops result in fast and low convergence, respectively (sometimes, high flows even oscillate without reaching a stationary solution). However, when high pressure drops are employed, the approximate vector **Ureduced_base** is very close to the final solution and the number of iterations in step 4 of the reduced basis method is very low. It means that we have to choose $\Delta P4$ thinking of the tradeoff between convergence and closeness to the solution in Eq. (4). In the case of the simulated larynx presented in this work, $\Delta P4=5$ Pa.

D. Coupling air and tissue systems

The links between both physical systems (air and tissue) are the airflow pressure and the moving mesh. As mentioned before, surface nodes of the airflow mesh are directly attached to surface nodes of the tissue nodes. It means that the air pressures are collected at the larynx walls and transferred to the tissue system in order to calculate the nodal displacement. Note that this direct node matching overcome problems of pressure estimation along the larynx walls because the pressures are exactly calculated over the tissue nodes.

The mesh updating also couples both systems because the change of airflow mesh generates a new velocity and pressure profiles along the laryngeal cavity. Again, moving together the airflow and tissue nodes located at the physical interface allows an easy information transfer.

E. Contact problem

The contact problem refers to the physical phenomena occurred when two or more bodies touch each other. In phonation, both true vocal folds collide according to the myoelastic-aerodynamic theory. Ishizaka and Flanagan (1972) changed the stress-displacement curve during the collision instant in order to avoid the penetration among the bodies. They also assumed that such phenomena always took place at the middle larynx section due to the laryngeal symmetry.

Alipour *et al.* (2000) considered a different approach: when their true vocal fold reached the middle section, they simply removed one degree of freedom of the collided node. Different from Ishizaka and Flanagan (1972), they did not apply the required force to avoid the body penetration. Apparently Gunter (2003) used a similar procedure to the method that will be described in the next paragraphs.

This simulation uses an algorithm (Bathe, 1996) to deal with the contact problem: all collided nodes (only the ones located at the tissue surface) are collected in order to calculate the required forces to avoid body interpenetration. The fundamental aspect is that such forces are calculated considering how deep one vocal fold can enter into each other.

Mathematically the following restrictions are kept for all surface tissue nodes (using contact problem notation):

$$G=(\mathbf{X}-\mathbf{Y})^T*\mathbf{N}\geqq 0$$
$$L=\mathbf{F}*\mathbf{N}\geqq 0 \qquad (5)$$
$$G*L=0.$$

It means that the gap (G) between two nodes ($\mathbf{X}$ and $\mathbf{Y}$ are the spatial position of master and slave nodes at different bodies) should be non-negative and that the collision force $\mathbf{F}$ should always take the bodies apart. The last restriction in Eq. (5) indicates that both the inequalities are exclusive: when one condition is reached, the other one is automatically equal to zero. Further theoretical details are found in Bathe (1996).

To add Eq. (5) into the linear system of equations produced by FEM to the tissue, the mathematical procedure described by Narayanaswamy (1985) is followed where the coupling of both FEM equations and collision restrictions are not necessary. In this procedure the restriction forces associated with the collided nodes are computed and then the tissue displacements under collision restrictions are calculated.

Therefore the algorithm to compute the tissue displacement in a specific time step is as follows:

1. Calculate the displacements without collision restrictions
2. While there are some body penetration:
2.1. Verify possible nodal collisions
2.2. Calculate the force collisions and nodal displacements according to Narayanaswamy (1985) under Eq. (5).
2.3. End while

The procedure is iterative because it is not known, *a priori*, which nodes will collide with some larynx surface, resulting in a nonlinear behavior to the contact problem. It can be realized that the contact problem is part of the tissue model. Therefore, the time step is only increased after the calculation of the nodal tissue displacements under collision restrictions.

As shown, the larynx symmetry is not used to simplify or reduce computational efforts. It means that the concept of master-slave bodies is not directly employed because there is

TABLE I. Geometric description of a simulated normal larynx.

Section	Center (cm)	Radius R1, R2, R3, R4 (cm)
S0	0, 0, −2	0.7, 0.7, 0.7, 0.7
S1	0, 0, −1	0.7, 0.7, 0.7, 0.7
S2	0, 0, −0.8	0.7, 0.7, 0.7, 0.7
S3	0, 0, −0.61	0.7, 0.6, 0.7, 0.6
S4	0, 0, −0.47	0.7, 0.25, 0.7, 0.25
S5	0, 0, −0.40	0.7, 0.075, 0.7, 0.075
S6	0, 0, −0.33	0.7, 0.025, 0.7, 0.025
S7	0, 0, −0.26	0.7, 0.025, 0.7, 0.025
S8	0, 0, −0.19	0.7, 0.025, 0.7, 0.025
S9	0, 0, −0.12	0.7, 0.025, 0.7, 0.025
S10	0, 0, −0.05	0.7, 0.025, 0.7, 0.025
S11	0, 0, 0	0.7, 0.235, 0.7, 0.235
S12	0, 0, 0.03	0.7, 0.35, 0.7, 0.35
S13	0, 0, 0.07	0.7, 0.5, 0.7, 0.5
S14	0, 0, 0.10	0.7, 0.515, 0.7, 0.515
S15	0, 0, 0.23	0.7, 0.45, 0.7, 0.45
S16	0, 0, 0.35	0.7, 0.46, 0.7, 0.46
S17	0, 0, 0.48	0.7, 0.6, 0.7, 0.6
S18	0, 0, 0.60	0.7, 0.7, 0.7, 0.7
S19	0, 0, 1.30	0.7, 0.7, 0.7, 0.7
S20	0, 0, 2	0.7, 0.7, 0.7, 0.7

Layer	Thickness (mm)	Sections
Cover	0.5	S5–S12
Ligament	0.5	S5–S12

no preferential body. All the surface nodes are tested against the tissue body to see if there is a collision and then the collided surface, which provides the normal **N** and position **Y** vectors in Eq. (5), is backtracked. This method is called two-way collision detection (ANSYS, 2000).

F. Final iterative procedure

After separately describing the mathematical algorithms for both physical systems, they are put together in an iterative loop in order to simulate the larynx as follow:

(1) Collect air pressures.
(2) Calculate tissue displacements verifying vocal fold collisions.
(3) Update tissue mesh.
(4) Update airflow mesh.
(5) Calculate airflow velocities and pressures.

Note that in the first iterative step, the collected air pressures are null.

G. Description of larynx parameters

Here the parameters used to simulate the larynx will be presented. The geometric description of the simulated larynx is shown in Table I. As mentioned before, the larynx is ''sliced'' into sections using ellipses for geometric definition.

The airflow parameters for simulation are $\mu_f\,(\text{viscosity}) = 1.79e\text{-}5$ Pa.s and $\rho_f\,(\text{density}) = 1.23\,\text{kg/m}^3$. The inflow and outflow air pressure are respectively set to 0.8 and 0 (zero) kPa. As in Alipour *et al.* (2000), the tissue layers have transversal isotropic elastic behavior. Therefore six viscoelastic parameters are needed: transverse and longitudinal Poisson's ratios (ν and ν'), transversal and longitudinal Young's modulus (E and E') and longitudinal shear modulus (μ'_m) and tissue viscosity η. Transversal shear modulus is not necessary because it is directly related to E and ν by

$$\mu_m = E/(2*(1+\nu)). \tag{6}$$

Alipour *et al.* (2000) defined $\nu' = 0$ because they eliminated any longitudinal movement. Here non-null longitudinal Poisson's ratios are allowed because all tissue nodes are free to move (except when they are under collision or boundary condition restrictions). This additional degree of freedom in the tissue specifications requires care in order to control the almost incompressible behavior of the laryngeal tissues. In order to simplify the model, all analyses are conducted by assuming $\nu = \nu'$. The final value is then chosen in order to reach almost incompressible tissues. Titze and Strong (1975) and Berry and Titze (1996) provide more details about this mechanical parameter.

TABLE II. Description of the viscoelastic tissue parameters of a normal larynx.

Tissue	E (kPa)	ν	E' (kPa)	μ'_m (kPa)	ν'	η (Pa.s)
Cover	2	0.76	20	20	0.76	1
Ligament	4	0.68	20	40	0.68	1
Body	20	0.45	20	30	0.45	15

Table II shows the values of tissue parameters for a specific simulation. Different from Alipour *et al.* (2000) the tissue viscosity of the body is set high according to observations of Titze and Strong (1975) where the authors discussed the similarities in the organic composition of the larynx tissues and other tissue tissues in the human body. Mathematically it establishes a critically damped system for the body tissues to quickly reach their stationary position. Lowering such a parameter brings the tissue to an under-damped condition and therefore an initial transitory oscillation is observed.

The transversal Young's modulus (E) is defined according to Tran *et al.* (1993) who measured it *in vivo*. Because their estimation resulted from the whole vocal fold reaction to an applied force, a fixed value is just extended for all the tissue layers. The other parameters are described in Berry and Titze (1994), Titze and Strong (1975), and Titze and Talkin (1979).

III. RESULTS AND DISCUSSIONS

Two analyses are done in order to demonstrate the effectiveness of the proposed model. First, the larynx geometries are fixed in three different profiles and the pressure distribution are calculated and compared with other models. Second, dynamic analyses are conducted to verify the effects of changing viscoelastic parameters and subglottal pressure on the synthesized glottal signal.

A. Airflow in fixed laryngeal geometries

During phonation, the human larynx roughly assumes three different shapes: divergent, convergent, and parallel. In each condition, there are variations according to the attack

TABLE III. Geometric description of larynxes in divergent, convergent, and parallel profiles. Only the differences from Table I are presented.

Profile	Section	Center (cm)	Radius R1, R2, R3, R4 (cm)
Divergent	S6	0, 0, −0.33	0.7 0.025 0.7 0.025
	S7	0, 0, −0.26	0.7 0.035 0.7 0.035
	S8	0, 0, −0.19	0.7 0.045 0.7 0.045
	S9	0, 0, −0.12	0.7 0.055 0.7 0.055
	S10	0, 0, −0.05	0.7 0.065 0.7 0.065
Convergent	S6	0, 0, −0.33	0.7 0.065 0.7 0.065
	S7	0, 0, −0.26	0.7 0.055 0.7 0.055
	S8	0, 0, −0.19	0.7 0.045 0.7 0.045
	S9	0, 0, −0.12	0.7 0.035 0.7 0.035
	S10	0, 0, −0.05	0.7 0.025 0.7 0.025
Parallel	S6	0, 0, −0.33	0.7 0.025 0.7 0.025
	S7	0, 0, −0.26	0.7 0.025 0.7 0.025
	S8	0, 0, −0.19	0.7 0.025 0.7 0.025
	S9	0, 0, −0.12	0.7 0.025 0.7 0.025
	S10	0, 0, −0.05	0.7 0.025 0.7 0.025

and entrance angles and the channel length. The glottal geometry shown in Table I was changed in order to produce such profiles. Table III shows only these modified sections and Fig. 3 presents theses geometric profiles in transversal view.

The subglottal pressure is 0.5884 kPa (or 6 cmH_2O) which is close to that provided by Guo and Scherer (1993). In their studies, a parabolic velocity profile was set in order to excite the airflow through their simulated larynx. Also, their profiles only considered one vocal fold, while in this work, the whole larynx (including the laryngeal ventricle and both false vocal folds) are geometrically represented.

Figure 4 shows the air pressure distribution along the whole larynx. In Guo and Scherer's two-dimensional larynxes, the pressures were directly extracted from the nodes in contact with the larynx walls. Because the proposed model uses a three-dimensional larynx, it is first divided into two halves, then the pressures are collected along the intersection of a coronal plane with one-half of the larynx.

These results are quite similar to the ones produced by Guo and Scherer (1993). The differences between the two approaches are related to the fact that the here simulated larynx is coarser than the actual one used by Guo and Scherer (1993). Increasing the mesh nodes would surely smooth the pressure distribution.

The maximum pressure gradient occurs just after the larynx section with minimal constriction. It is developed in the glottal entrance for divergent and parallel profiles and in the glottal output for convergent profiles.

It is possible to observe a secondary negative pressure region formed over the glottal walls becoming more evident although it is less intense (in magnitude) than the main negative pressure region (the same phenomenon is observed when the number of nodes in the airflow mesh is doubled—the result is just smoother then that obtained with the original mesh). When the true vocal fold diameters are increased by 0.02 cm, the pressure distribution becomes smoother.

This phenomenon occurs because tiny glottises cause large vortexes after large aerodynamic jumps (represented by the larynx) due to the demands of fluid incompressibility and convection. Consequently, the transglottal pressure drop is increased when the glottal diameter is reduced.

It was also observed that the longitudinal distribution of air pressure is not constant. The central portion of the vocal folds (approximately 50% of the glottis) is more affected by the air pressure gradient. This fact explains the horizontal phase difference in the vocal fold movements. Because the pressure in the anterior and posterior comissures is very low, it seems that the movements of these glottal regions are not

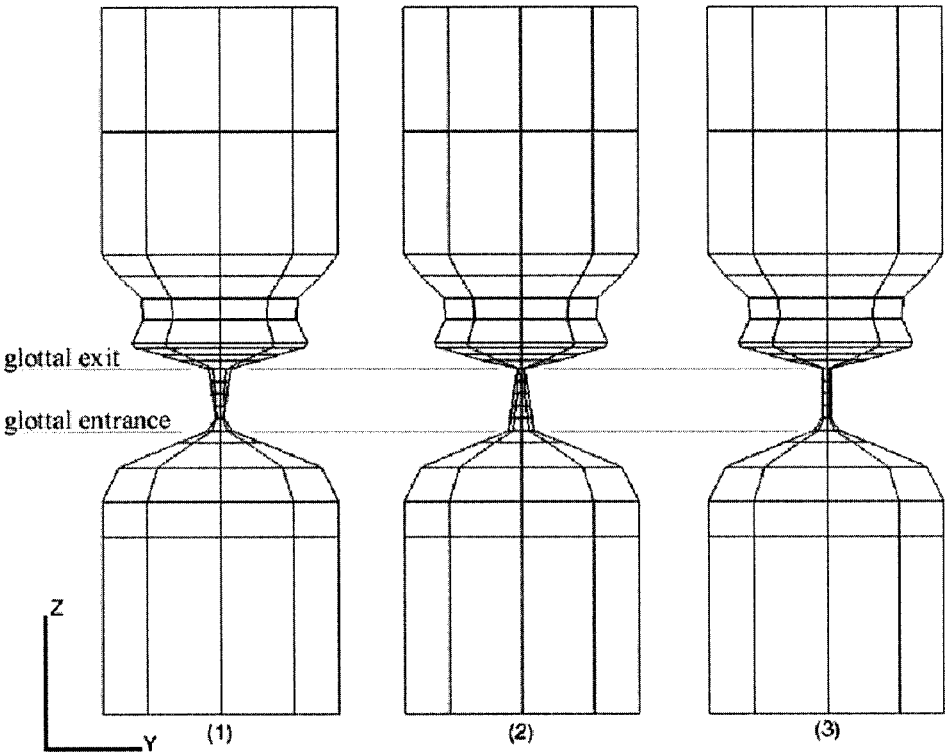

FIG. 3. Geometric description of larynxes with (1) divergent, (2) convergent, and (3) parallel profiles in transversal view.

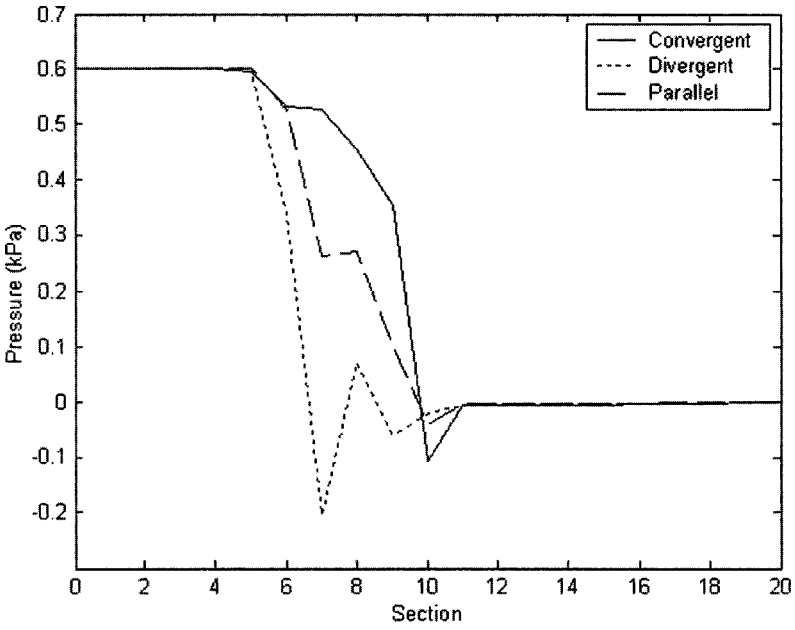

FIG. 4. Pressure distribution over the surface of larynxes with divergent, convergent, and parallel profiles.

excited by aerodynamic conditions (suction, for example) but by influence of the movements of the central portion of the true vocal folds.

The false glottal folds also change pressure distribution. Reducing their diameters increases the air pressure gradient along the larynx. Specifically negative pressures become ''more negative.'' Although this phenomenon happens for all three geometric profiles, the relationship between false vocal fold area and pressure gradient change is nonlinear. To clarify these findings, Fig. 5 shows the differences between three larynx configurations with divergent profiles where the geometry of the false vocal folds have changed. The geometry of all these larynxes is presented in Table IV.

The reduction of the laryngeal areas formed by the false vocal folds increases the transglottal pressure drop. Similar results are obtained for parallel and convergent laryngeal profiles. This phenomenon helps to understand how whispered voices are sustained. A simultaneous reducing of subglottal pressure and false vocal fold area allows the larynx to keep the true vocal folds vibrating, as demonstrated by Miller *et al.* (1988). It means that the minimum subglottal pressure condition to excite the self-vibration of the larynx during the phonation should consider the false vocal fold area at extremely low pressure drops.

B. Complete simulation

All simulations start with a larynx whose geometry is shown in Table I. The viscoelastic properties of the laryngeal tissues are presented in Table II. The lung pressure was 0.8 kPa. Different from Alipour *et al.* (2000), whose simulation was just restricted to one true vocal fold, the present model considered the whole larynx.

Figure 6 presents the synthesized glottal signal whose values are obtained by integrating the volumetric velocity along the exit laryngeal surface. Note the initial transient and

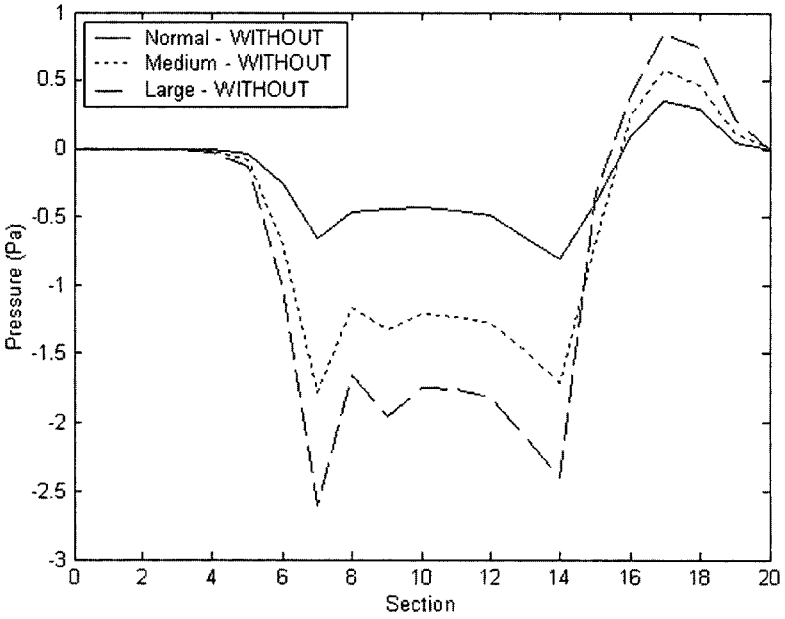

FIG. 5. Curves representing the difference between the pressure distribution of larynxes with three different false vocal fold shapes (normal, medium, and large) and the pressure distribution of a larynx without such a structure. All these larynxes have a divergent profile.

TABLE IV. Geometric description of larynxes with four different false vocal fold shapes which have divergent profiles.

Type of false vocal folds	Section	Center (cm)	Radius R1, R2, R3, R4 (cm)
"None"	S14	0, 0, 0.10	0.7 0.6 0.7 0.6
	S15	0, 0, 0.23	0.7 0.7 0.7 0.7
	S16	0, 0, 0.35	0.7 0.7 0.7 0.7
	S17	0, 0, 0.48	0.7 0.6 0.7 0.6
"Normal"	S15	0, 0, 0.23	0.7 0.45 0.7 0.45
	S16	0, 0, 0.35	0.7 0.46 0.7 0.46
"Medium"	S15	0, 0, 0.23	0.7 0.35 0.7 0.35
	S16	0, 0, 0.35	0.7 0.36 0.7 0.36
"Large"	S15	0, 0, 0.23	0.7 0.25 0.7 0.25
	S16	0, 0, 0.35	0.7 0.26 0.7 0.26

rising of volume velocity until becomes a stationary.

The calculated fundamental frequency is 164 Hz, which is higher than the one presented by Alipour *et al.* (2000). The open quotient for this simulation is 0.6347 while Alipour *et al.* (2000) reported 0.9000. The temporal variables are calculated for the last nine glottal signal cycles when the signal became steady. The difference between the quantities obtained in both simulations can be attributed to the viscoelastic and geometric property differences. It should be taken into account that the three-dimensional aspect of the proposed model affects the pressure distribution along the vocal folds, as demonstrated before, and causes a horizontal phase difference in the tissue movements. It seems that the presented larynx has more mass and therefore more inertial energy than Alipour's one, even considering the differences across the tissue viscosity properties (especially in body tissue specification). This additional inertial energy surely contributed to lower the open quotient value when compared to that obtained by Alipour *et al.* (2000).

Lung pressure affects the temporal properties of the glottal signal. Figure 7 shows the volumetric velocity curves for three larynxes excited by different lung pressures (0.7, 0.8, and 0.9 kPa). The open quotients obtained from these glottal signals are 0.6747, 0.6347, and 0.6249. The lung pressure increase causes higher extensions in the cover tissue movements and, consequently, higher kinetic energy. It means that the glottal closing interval becomes higher because the time of kinetic energy dissipation by the collision effects is increased. Therefore the open quotient is decreased.

The fundamental frequency of each glottal signal is 167.4, 164.0, and 161.3 Hz, showing a variation of −21 Hz/kPa from 0.7 to 0.8 kPa and −34 Hz/kPa from 0.8 to 0.9 kPa. The absolute values are quite similar to the 20.3943 to 30.5915 Hz/kPa (or 2 to 3 Hz/cmH_2O) ratio presented by Ishizaka and Flanagan (1972). However, this ratio is inversely proportional to lung pressure: an increase in lung pressure produces a decrease in the fundamental frequency.

However, the aerodynamic effects in fundamental frequency changes when the larynx become stiffer. Using a larynx with same geometry and higher transversal Young's constants for cover and ligament tissues, as shown in Table V, an increase of 1.5 Hz in the fundamental frequency when the lung pressure is increased from 0.8 to 0.9 kPa is produced. Figure 8 shows that this stiffer larynx excited by 0.8 and 0.9 kPa produces glottal signals with 188.8 and 190.3 Hz, respectively.

Such a dependence of the lung pressure versus fundamental frequency ratio to the laryngeal tissue stiffness (or viscoelastic properties, in a more general view) presents interesting questions on the interrelationship between both myoelastic and aerodynamic aspects of the vocal fold vibration. The results demonstrate that this ratio is nonlinear and dependent on tissue mechanics, although this ratio is quite similar to the ones presented by Ishizaka and Flanagan (1972) in their two-mass model.

Another important aspect is the larynx spatial movements. Alipour *et al.* (2000) presented the coordinates of a tissue point during a phonation, showing that the larynx movements are also periodic. Figure 9 shows the studied spatial points whose coordinates were extracted during a

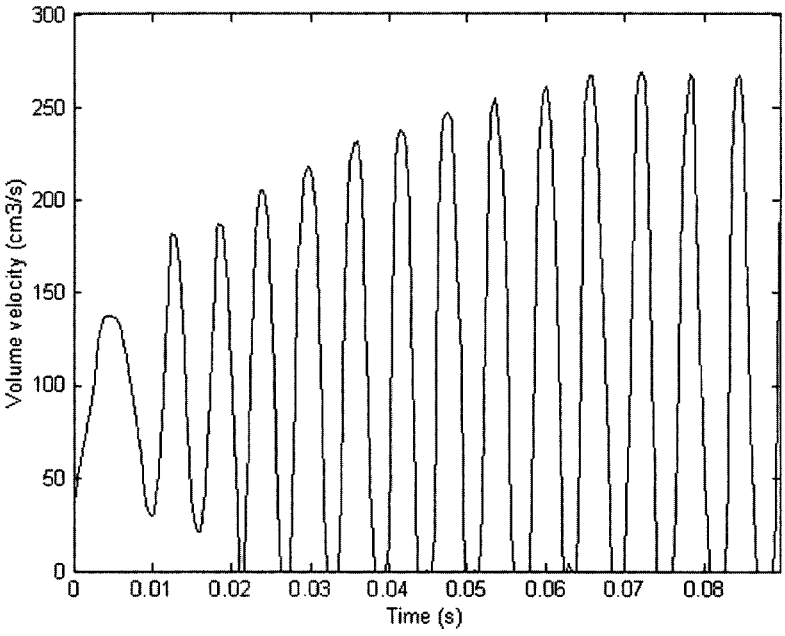

FIG. 6. Glottal signal obtained from a normal larynx excited by pressure drop of 0.8 kPa.

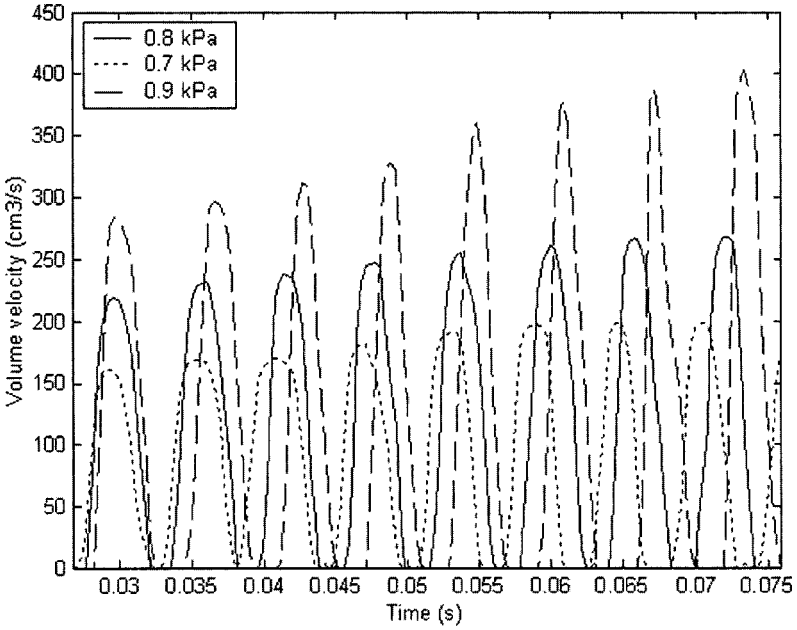

FIG. 7. Glottal signals obtained from normal larynxes excited by different pressure drops.

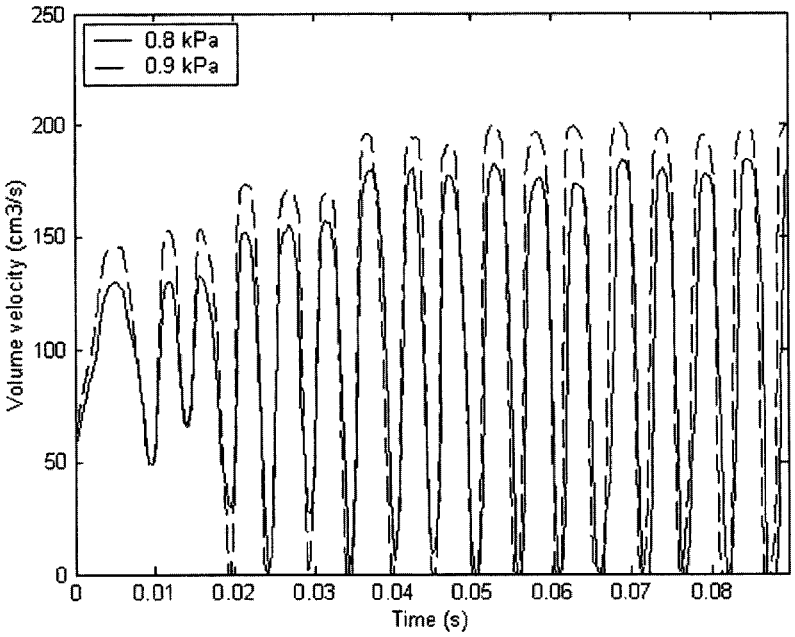

FIG. 8. Glottal signals obtained from stiffer larynxes excited by different pressure drops.

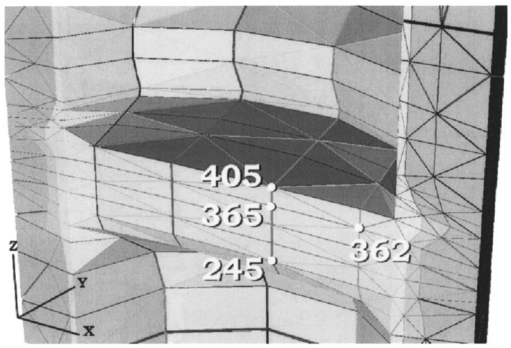

FIG. 9. Nodes whose movements are tracked along the time.

TABLE V. Description of the viscoelastic tissue parameters of a stiff larynx (specifically the transversal Young's module E for all tissues are higher than the ones presented for a normal larynx as described in Table II).

Tissue	E (kPa)	ν	E' (kPa)	μ_m' (kPa)	ν'	η (Pa.s)
Cover	3	0.73	200k	200k	0.73	1
Ligament	5	0.66	20	40	0.66	1
Body	20	0.45	20	30	0.45	15

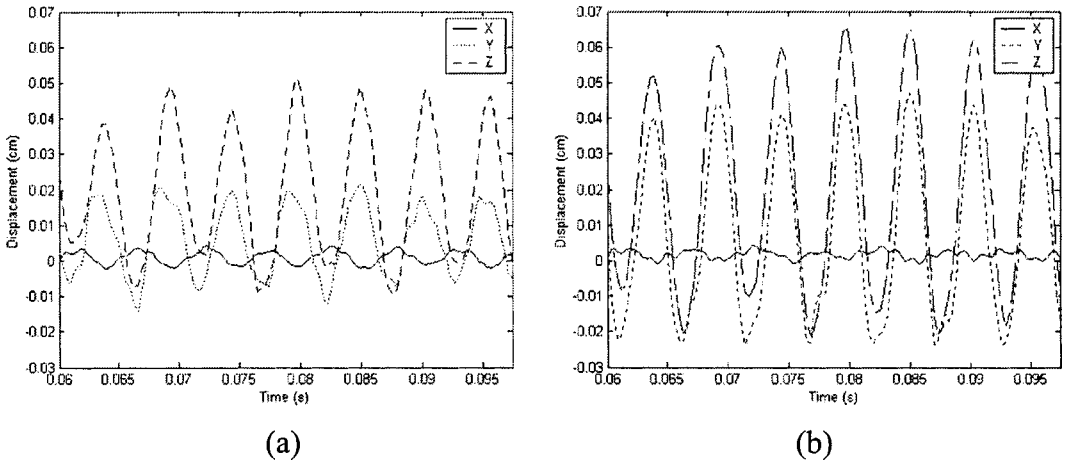

FIG. 10. Displacement of the nodes (a) 365 and (b) 405 along the three Cartesian axes.

complete simulation of the larynx with mechanical properties described in Table V.

Analyzing the coordinates of the points 365 and 405 (Fig. 10) the surface tissues near the glottal exit have higher amplitude than those near the glottal entrance. Considering that the mathematical modeling of the laryngeal tissues assumes that there is movement along the longitudinal axes, both points show displacements along this direction. Alipour *et al.* (2000) assumed such the movements in longitudinal direction are insignificant, allowing a reduction of mathematical complexity in their tissue modeling. Clearly their assumptions are correct, especially for the region near the glottis exit. However, the magnitudes along the three Cartesian axes becomes smaller as the distance from the glottis center becomes larger.

The periodicity degree seems to be higher for surface points located near the glottis exit. It can be related to the movement amplitude at that region. For nodes located far from the glottal exit, high-frequency components found in the longitudinal movements are no more insignificant in comparison with the movements in all other axes.

Additionally, an analysis of Fig. 11 reveals that the phase difference in the horizontal movement of the vocal folds are close to zero. This result is also found in Gunter (2003). The movement amplitudes of nodes 362 and 365 confirm that the main tissue displacements occur in the central portion of the vocal folds, which is caused by the pressure drop magnitude at this region.

Figure 12 shows that the movement of different points of vocal folds can present significant vertical phase difference in their movements. Concurrently with Fig. 11, movements in the *Y* direction are almost in-phase for the nodes 245, 365, and 405. Figure 12 clearly shows approximately 90° phase difference between nodes 245 and 405 in the *Z* direction. It is interesting to note that node 245 presents a curve whose its rise time is shorter than its fall time in the *Y* direction. This characterize the wavy behavior of the surface of vocal folds found in laryngoscope videos. These phenomena happen because node 245 is influenced by two concurrent forces: an aerodynamic force that always pushes it upward and a tissue force that is caused by the movements of nodes like 365 and 405. Therefore, the location where the vertical phase difference is a nonlinear function of mechanical and geometric properties of the laryngeal tissues and aerodynamic forces produced in phonation.

Considering the movement extension, the cover tissue of nodes at glottal exit (like node 405) suffers more compression and expansion then other laryngeal tissues. Gunter (2003) reports that collision forces acting at this node can be responsible for damages in tissue structures. The present re-

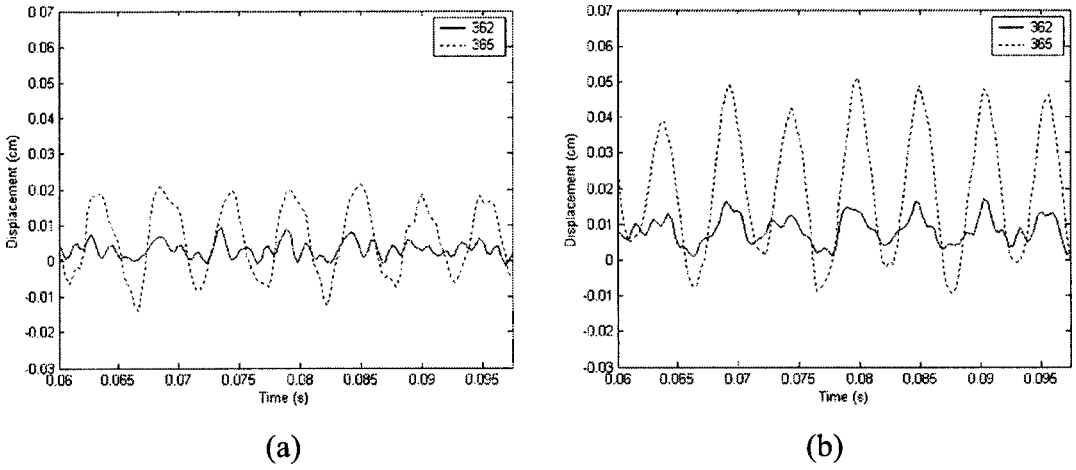

FIG. 11. Displacement of the nodes 362 and 365 along (a) *Y* and (b) *Z* directions.

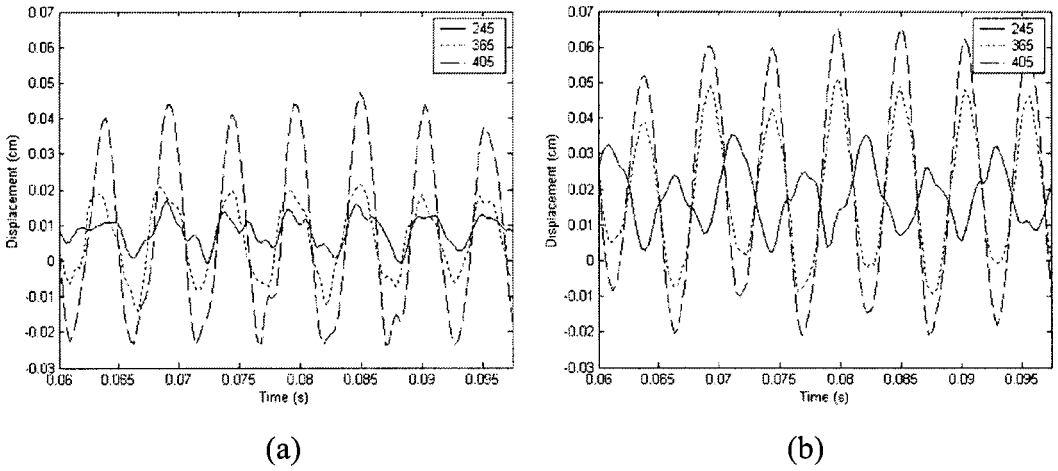

FIG. 12. Displacement of the nodes 245, 365, and 405 along (a) *Y* and (b) *Z* directions.

sults indicate that the large movements of glottal exit nodes can be a source of alterations in larynx tissues. It is important to consider that in phonatory conditions where both vocal folds barely reach each other, like in high-pitch voices, it is not the collision forces that are the cause for tissue damages (specially the superficial tissue layer of lamina propria) but the extreme nodal displacements as a consequence of high longitudinal and transverse stretch and aerodynamic forces.

In several larynx simulations, an additional phenomenon is observed: an incomplete glottal closure. Two spaces, located at both anterior and ''posterior'' comissures, are formed during the ''glottal closure'' time interval. These spaces are pointed by arrows in Fig. 13. These openings happen due to the incapacity of the aerodynamic forces to displace the laryngeal tissue located there during the phonation. Section III A shows that the air pressure applied over the larynx tissues is not constant and the main aerodynamic force is exerted over the central portion of the true vocal folds. Therefore, parts of these structures move first, bringing along comissure tissues. But this continuum effect is not enough to close the whole glottis. It is important to emphasize that the term ''posterior'' comissure refers to the point where both arythenoid cartilages meet each other during the phonatory process. By the fact that the present model is not representing all details—geometric and mechanical—of the larynx structures, careful consideration should be taken in order to analyze the presence of air leakage at ''posterior'' comissure.

Pelorson *et al.* (1994) considered such an incomplete closure in their model and mentioned that more realistic voices, from a perceptual view, are obtained when such airflow leakage is taken into account. As shown, the three-dimensional model presented here is able to reproduce such phenomena.

IV. CONCLUSIONS

This work presents the simulation of three-dimensional larynx models using the finite-element method as the main mathematical framework. The simulated models include false vocal folds and laryngeal ventricles which are first introduced in numeric simulation of larynx. The results show that these laryngeal structures affect the pressure distribution along the glottal walls and therefore modify the final glottal waveform.

The airflow velocities and pressures are obtained by numerically solving Navier–Stokes equations at each time step after the airflow mesh update. Mathematical strategies are used to speed up and control the convergence of the iterative methods employed to solve the sets of nonlinear equations. Different from Guo and Scherer (1993) and following Ishizaka and Flanagan (1972), the airflow is excited by a pressure drop.

Linear models describe the laryngeal tissues as Alipour *et al.* (2000). However, the collision between both true vocal folds during the glottal closure is modeled by calculating the surface forces that avoid the interpenetration between both tissues. This is the first time that this mathematical method is

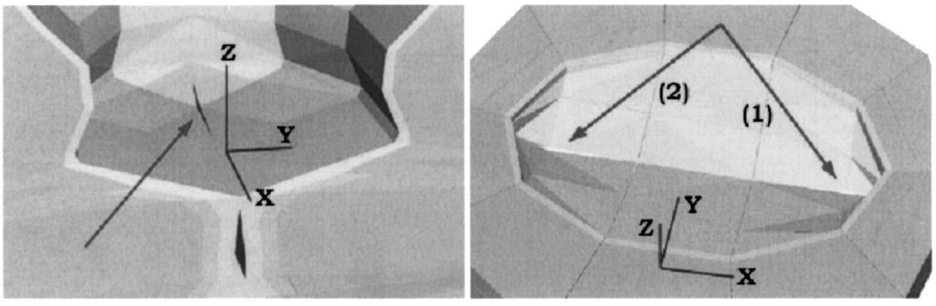

FIG. 13. Incomplete closure of the larynx: (a) at the ''posterior'' comissure and (b) at both the (1) anterior and (2) ''posterior'' comissures.

incorporated in whole larynx simulation under phonatory conditions although it is currently employed in mechanic computation.

The larynx meshes (both airflow and laryngeal tissues) are constructed by using hyper-ellipes. This method allows researchers to reconstruct larynx models in straightforward manner and reproduce the presented results. More realistic geometries can be obtained by manual manipulation of the larynx nodes or by automatic scanning of MRI images along with sophisticated automatic mesh generators.

Horizontal and vertical phase difference in the glottal tissue movements are captured by the larynx model and physically they are caused by the nonlinear air pressure distribution along the laryngeal surfaces and the viscoelastic constitution of the larynx tissues (specially in the glottal cavity).

Incomplete glottal closure during phonation are observed in some simulations, around anterior and posterior comissures. This phenomena is more evident in larynx with large glottal areas and/or with stiffer tissues. Pelorson *et al.* (1994) state that airflow escapes during phonation make the voice signal more perceptually realistic.

The lung pressure to fundamental frequency ratios obtained in the simulations with the present model are quite similar to the ones presented by Ishizaka and Flanagan (1972). However, the results show that these ratios are dependent on viscoelastic properties of the laryngeal tissues.

Statically the airflow for the three most significant laryngeal profiles are solved and the nonlinear behavior of the pressure distribution formed over the larynx walls justifies the vocal fold movements. The volume velocities are lower than the ones presented by Guo and Scherer (1993) due to the three-dimensional aspect of the larynx models presented here. In addition to the transversal funneling of the airflow along the larynx, there is another airflow funneling in sagittal plane. It is caused by the finite aspect of true three-dimensional larynxes and glottis shape which gets narrower in the direction of both comissures.

The next steps in larynx simulations require some model improvements. Larynx airflow and tissue meshes with higher numbers of nodes have to be used in order increase the accuracy of simulations although the inherit computational power expenses.

Additionally, sophisticated models to describe the viscoelastic nature of the larynx tissues should be studied, with special emphasis to their fibrous aspect. We believe that this is a key study that will bring more realistic results to the larynx simulations.

Another important aspect to improve the present model is to incorporate the airflow unsteady aspect into Navier–Stokes equations. The airflow mesh deforming also has to be put into the final partial differential equations in order to correctly compute the airflow velocities and pressures along the larynx. Work is ongoing to incorporate this missing aerodynamic aspect into the simulation model.

ACKNOWLEDGMENTS

This work was supported by FAPESP (The State of São Paulo Research Foundation, Brazil).

ANSYS (**2000**). *ANSYS 5.7 Theory Reference* (Ansys, Canonsburg).
Alipour, F., Berry, D., and Titze, I. (**2000**). ''A finite-element model of vocal-fold vibration,'' J. Acoust. Soc. Am. **108**, 3003–3012.
Bathe, K. (**1996**). *Finite Element Procedures* (Prentice–Hall, Upper Saddle River, NJ).
Berry, D., and Titze, I. (**1996**). ''Normal modes in a continuum model of vocal fold tissues,'' J. Acoust. Soc. Am. **100**, 3345–3354.
Berry, D., Herzel, H., Titze, I., and Krischer, K. (**1994**). ''Interpretation of biomechanical simulations and chaotic vocal fold oscillations with empirical eigenfunction,'' J. Acoust. Soc. Am. **95**, 3595–3604.
De Vries, M., Schutte, H., and Verkerke, G. (**1999**). ''Determination of parameters for lumped parameter models of the vocal folds using a finite-element method approach,'' J. Acoust. Soc. Am. **106**, 3620–3628.
Deblois, B. (**1996**). ''Quadratic, streamline upwinding for finite element method solutions to 2-D convective transport problems,'' Comput. Methods Appl. Mech. Eng. **134**, 107–115.
Demmel, J., Eisenstat, S., Gilbert, J., Li, X., and Liu, J. (**1999**). ''A supernodal approach to sparse partial pivoting,'' SIAM J. Matrix Anal. Appl. **20**, 720–755.
FIDAP (**1999**). *FIDAP 8 Theory Manual* (Fluent, Lebanon).
Gresho, P., and Sani, R. (**1998**). *Incompressible Flow and the Finite Element Method: Advection-diffusion and Isothermal Laminar Flow* (Wiley, Chichester).
Gunter, H. (**2003**). ''A mechanical model of vocal-fold collision with high spatial and temporal resolution,'' J. Acoust. Soc. Am. **113**, 994–1000.
Guo, C., and Scherer, R. (**1993**). ''Finite element simulation of glottal flow and pressure,'' J. Acoust. Soc. Am. **94**, 688–700.
Hirsch, C. (**1988**). *Numerical Computation of Internal and External Flows* (Wiley, Chichester), Vol. 2.
Huebner, K., and Thornton, E. (**1982**). *The Finite Element Method for Engineers* (Wiley, New York).
Ishizaka, K., and Flanagan, J. (**1972**). ''Synthesis of voiced sounds from a two-mass model of the vocal cords,'' Bell Syst. Tech. J. **51**(6), 1233–1268.
Johnson, A., and Tezduyar, T. (**1994**). ''Mesh update strategies in parallel finite element computations of flow problems with moving boundaries and interfaces,'' Comput. Methods Appl. Mech. Eng. **119**, 73–94.
Miller, J., Pereira, J., and Thomas, D. (**1988**). ''Fluid-flow through the larynx channel,'' J. Sound Vib. **121**, 277–290.
Narayanaswamy, O. (**1985**). ''Processing nonlinear multipoint constraints in the finite element method,'' Int. J. Numer. Methods Eng. **21**, 1283–1288.
Pelorson, X., Hirschberg, A., van Hassel, R. R., Wijnands, A. P. J., and Auregan, Y. (**1994**). ''Theoretical and experimental study of quasisteady-flow separation within the glottis during phonation. Application to a modified two-mass model,'' J. Acoust. Soc. Am. **96**, 3416–3431.
Peterson, J. (**1989**). ''The reduced basis method for incompressible viscous flow calculations,'' SIAM (Soc. Ind. Appl. Math.) J. Sci. Stat. Comput. **10**, 777–786.
Sampaio, P. (**1991**). ''A Petrov-Galerkin formulation for the incompressible Navier-Stokes equations using equal order interpolation for velocity and pressure,'' Int. J. Numer. Methods Eng. **31**, 1135–1149.
Sani, R. L. and Gresho, P. M. (**1994**). ''Resume and remarks on the open boundary condition minisymposium,'' Int. J. Numer. Methods Fluids **18**, 1135–1149.
Tabata, M., and Fujima, S. (**1991**). ''An upwind finite element scheme for high-Reynolds-numfer flows,'' Int. J. Numer. Methods Fluids **12**, 305–322.
Titze, I., and Strong, W. (**1975**). ''Normal modes in vocal cord tissues,'' J. Acoust. Soc. Am. **57**, 736–744.
Titze, I., and Talkin, D. (**1979**). ''A theoretical study of the effects of various laryngeal configurations on the acoustics of phonation,'' J. Acoust. Soc. Am. **66**, 60–74.
Tran, Q., Gerratt, B., Berke, G., and Kreiman, J. (**1993**). ''Measurement of Young's modulus in the in-vivo human vocal folds,'' Ann. Otol. Rhinol. Laryngol. **102**, 584–591.